

# SHAPE OPTIMIZATION UNDER A CONSTRAINT ON THE WORST-CASE SCENARIO

FABIEN CAUBET\*, MARC DAMBRINE\*, GIULIO GARGANTINI\*<sup>†</sup>, AND JÉRÔME MAYNADIER<sup>†</sup>

**Abstract.** This work falls within the general framework of robust shape optimization: a physical parameter of the problem is poorly known. In the model case studied, we try to minimize the volume of an elastic structure subjected to uncertain loading under mechanical constraints: compliance or a von Mises stress norm must remain controlled. We study two approaches: the first consists in reducing the problem to a multiple loading type, while the second is based on a Clarke sub differential calculation. Our contributions are a theoretical convergence result for the first approach and a numerical comparison of the two approaches on test cases.

**Key words.** shape optimization under uncertainties, worst-case optimization, robustness, convexity, subdifferential, shape derivatives.

**1. Introduction.** In this work we focus on the optimization of linear elastic structures subjected to uncertain mechanical loads. Several different approaches can be contemplated in order to take uncertain parameters into account. If some information on the probability distribution of the uncertainties is available, techniques of Robust Topology Optimization (RTO) or Reliability-Based Topology Optimization (RBTO) can be considered. See [28, 14, 3, 18, 21, 19] for more information on the different approaches to RTO and RBTO problems. As reported in [11], the optimization of the worst-case scenario is preferable to other approaches involving stochastic quantities when the data are imprecise or if they are uncertain with an unknown probability distribution, or if the strict respect of the constraint in all circumstances is of primary importance. In many industrial applications, safety is a critical issue and the strict respect of the constraint in all circumstances is of primary importance. Any probabilistic criterion to measure the risk of failure cannot be used in this context. Therefore, in this paper we focus on a worst-case criterion.

*Problem statement.* Let us study the following shape optimization problem, where the objective consists in the minimization of the volume of the structure under mechanical constraints. We consider a structure represented by a Lipschitz continuous bounded domain  $\Omega \subset \mathbb{R}^d$ , with  $d = 2$  or  $d = 3$ . We suppose that its boundary  $\partial\Omega$  to be divided in three disjoint parts with strictly positive measure:  $\Gamma_D$ ,  $\Gamma_N$  and  $\Gamma_0$ . The structure is clamped in  $\Gamma_D$ , and a force  $\mathbf{g}$  is applied on  $\Gamma_N$ . The displacement solves the following linear elasticity equations:

$$(1.1) \quad \begin{cases} -\operatorname{div}(\boldsymbol{\sigma}(\mathbf{u}_{\Omega, \mathbf{g}})) &= \mathbf{f} & \text{in } \Omega, \\ \boldsymbol{\sigma}(\mathbf{u}_{\Omega, \mathbf{g}}) \mathbf{n} &= \mathbf{g} & \text{on } \Gamma_N, \\ \boldsymbol{\sigma}(\mathbf{u}_{\Omega, \mathbf{g}}) \mathbf{n} &= \mathbf{0} & \text{on } \Gamma_0, \\ \mathbf{u}_{\Omega, \mathbf{g}} &= \mathbf{0} & \text{on } \Gamma_D. \end{cases}$$

Here  $\boldsymbol{\sigma}(\mathbf{u}_{\Omega, \mathbf{g}})$  denotes the stress tensor which is taken, according to Hooke's law, as a linear function of the linearized strain tensor  $\boldsymbol{\varepsilon}(\mathbf{u}_{\Omega, \mathbf{g}})$  defined as the symmetric part of the gradient. For a homogeneous isotropic material, the linear relation between the

---

\*E2S UPPA, CNRS, LMAP, UMR 5142, Université de Pau et de Pays de l'Adour, Pau, 64000, France.

<sup>†</sup>Safran Helicopter Engines, Avenue Joseph Szydlowski, Bordes, 64510, France.

stress and strain tensors is given by

$$\boldsymbol{\sigma}(\mathbf{u}_{\Omega, \mathbf{g}}) = 2\mu\boldsymbol{\varepsilon}(\mathbf{u}_{\Omega, \mathbf{g}}) + \lambda(\operatorname{div} \mathbf{u}_{\Omega, \mathbf{g}})\mathbb{I},$$

where  $\mathbb{I}$  is the identity matrix, and  $\mu$  and  $\lambda$  are the Lamé parameters.

In this work, we assume that the mechanical loads applied are uncertain. Let us suppose that  $\mathbf{f}$  belongs to  $L^2(\Omega)^d$  and that  $\mathbf{g}$  is a parameter that belongs to a bounded set  $\mathcal{G} \subset L^2(\Gamma_N)^d$ . Then we consider the following generic constrained optimization problem defined on the set of admissible shapes  $\mathcal{S}_{\text{adm}}$  which will be specified below:

$$(1.2) \quad \left\{ \begin{array}{l} \text{Find the admissible shape } \Omega \in \mathcal{S}_{\text{adm}} \text{ minimizing the volume } \operatorname{Vol}(\Omega) \\ \text{under the constraint } \sup_{\mathbf{g} \in \mathcal{G}} H(\mathbf{u}_{\Omega, \mathbf{g}}, \Omega) \leq \tau, \\ \text{where the displacement } \mathbf{u}_{\Omega, \mathbf{g}} \in H_{\Gamma_D}^1(\Omega)^d \text{ solves (1.1).} \end{array} \right.$$

Here and in the following,  $\tau$  is a given threshold. Finally, we assume that the considered constraint functional  $H(\cdot, \cdot)$  is written in integral form as

$$(1.3) \quad H(\mathbf{u}, \Omega) = \int_{\Omega} (j_0(\mathbf{u}(\mathbf{x})) + j_1(\nabla \mathbf{u}(\mathbf{x}))) \, d\mathbf{x} \quad \text{for } \mathbf{u} \in H^1(\Omega)^d,$$

with  $j_0$  and  $j_1$  continuous functions. If the mapping  $\mathbf{g} \mapsto H(\mathbf{u}_{\Omega, \mathbf{g}}, \Omega)$  is continuous and the set  $\mathcal{G}$  is compact,  $H(\mathbf{u}_{\Omega, \mathbf{g}}, \Omega)$  reaches its supremum for some  $\mathbf{g} \in \mathcal{G}$ , and the constraint can be replaced by  $\max_{\mathbf{g} \in \mathcal{G}} H(\mathbf{u}_{\Omega, \mathbf{g}}, \Omega) \leq \tau$ .

*State of the art.* As remarked in [2], two different points of view can be adopted, according to whether the functional affected by the perturbation acts as the objective of an optimization problem or as a constraint. If the objective of the optimization is the minimization of the maximal possible level of a functional, the problem can be formulated as a *min-max* problem. This interpretation can also be applied to the case of constrained optimization problems where an upper bound on the maximum of a functional is imposed. However, this constraint can also be interpreted as imposing an upper bound on the constraining functional for all possible configuration of the uncertain parameters.

Different techniques to solve shape optimization problems with worst-case functionals have been proposed. In [16, 24, 33, 5] the objective of the optimization problem consists in minimizing the maximal possible value of a given functional. In particular, the studies of Cherkaev and Cherkaeva [16], and of Allaire and de Gournay [24] focus on minimizing the *robust compliance* of an elastic structure subject to an uncertain load by taking advantage of the convexity of that specific functional. In [29, 2, 5] are considered also problems where the uncertain functional acts as a constraint, and numerical examples are provided for density and level-set methods. The authors of [2] consider smooth functionals subject to small perturbations, and propose a method to compute the shape derivative of their supremum using linearization techniques. This approach was slightly improved in [22]. For further information about worst-case problems, outside the domain of structure optimization, we refer to [11, 10].

*Contribution and organization of the paper.* In this paper, two different methods for solving shape optimization problems under worst-case scenario constraints for a given functional are presented and compared. Contrarily to the approach of [2], no assumptions on the size uncertainties are asserted. However, both methods require the convexity of the constraint functional with respect to the displacement.

In industrial applications, the principal technique to approximate the solution of problem (1.2) consists in the identification of a number  $N$  of representative loading conditions and consider them as separate constraints of the shape optimization problem. In section 2 we study that method and provide our first contribution **Theorem 2.9**: as  $N$  goes to infinity, this approach provides a sequence of minimizers that converges to a domain solving the original problem. To do this, we assume convexity of both the constraint functional and the set of allowable mechanical loads. In section 3 we study a general approach based on Clarke's subdifferentials dealing with the non differentiability of a supremum. In that context, we provide in **Proposition 3.7** the expression of the shape subdifferential. Finally, in section 4 the results two methods are compared for some numerical applications in three dimensions.

**2. A multi-scenarios approach for the worst-case.** In this section, convexity is the essential tool that allows us to avoid making assumptions about the small amplitude of uncertainties. More precisely, we will use the fact that the ambiguous set for the loading is a convex compact set in a finite dimensional space and that the constraint is a convex function of the displacement.

**2.1. The chosen topology on sets and the continuity of the constraints.**

Before describing the first approach, we recall a classical result concerning the maximization of convex functionals on convex sets. Such result descends directly from [36, Theorem 32.3] and its corollaries.

**PROPOSITION 2.1.** *Let  $f : \mathcal{X} \rightarrow \mathbb{R}$  be a convex and bounded function defined on the vector space  $\mathcal{X}$ , and  $\mathcal{S} \subset \mathcal{X}$  a compact convex set. Then,  $f$  attains  $\sup_{\mathbf{x} \in \mathcal{S}} f(\mathbf{x})$  in at least a point  $\bar{\mathbf{x}} \in \mathcal{S}$ , belonging to the border  $\partial\mathcal{S}$  of the set  $\mathcal{S}$ . Moreover, if  $\mathcal{S}$  is a convex, closed, and bounded polyhedral set,  $\bar{\mathbf{x}}$  can be found among the vertices of  $\mathcal{S}$ .*

In order to define the concept of convergence for the domains, it is necessary to introduce a topology on the set of admissible shapes  $\mathcal{S}_{\text{adm}}$  and among the sets of possible mechanical loads. At first, we recall the notion of Hausdorff distance between subsets of metric spaces as in [31, Definition 2.2.7], see also [7, Proposition 1.2].

**DEFINITION 2.2 (Hausdorff distance).** *Let  $\mathcal{M}$  be a metric space provided with the distance  $d_{\mathcal{M}}$ , and let  $\mathcal{A}_1$  and  $\mathcal{A}_2$  be two compact subsets of  $\mathcal{M}$ . The Hausdorff distance between the sets  $\mathcal{A}_1$  and  $\mathcal{A}_2$  is*

$$d_{\text{H}}(\mathcal{A}_1, \mathcal{A}_2) = \max \left\{ \sup_{\mathbf{x} \in \mathcal{A}_1} d_{\mathcal{M}}(\mathbf{x}, \mathcal{A}_2), \sup_{\mathbf{y} \in \mathcal{A}_2} d_{\mathcal{M}}(\mathbf{y}, \mathcal{A}_1) \right\}.$$

In order to define a metric and the notion of convergence for open subsets of  $\mathcal{M}$ , we limit our study to uniformly bounded open sets. Let  $\mathcal{B} \subset \mathcal{M}$  be a fixed compact subset of  $\mathcal{M}$ . We can introduce a metric on the class of the open subsets of  $\mathcal{B}$  as proposed in [31, Definition 2.2.8 and Remark 2.2.10].

**DEFINITION 2.3 (Metric among open spaces and Hausdorff convergence).** *We consider the following function  $m_{\text{H}}$  defined on the class of subsets of  $\mathcal{B}$*

$$(2.1) \quad m_{\text{H}}^{\mathcal{B}}(\mathcal{A}_1, \mathcal{A}_2) = d_{\text{H}}(\mathcal{B} \setminus \mathcal{A}_1, \mathcal{B} \setminus \mathcal{A}_2).$$

*The function  $m_{\text{H}}$  defines a metric structure on the class of open subsets of  $\mathcal{B}$ . Moreover, if  $\hat{\mathcal{B}}$  is another compact subset of  $\mathcal{M}$ , and  $\mathcal{A}_1$  and  $\mathcal{A}_2$  are open sets contained in both  $\mathcal{B}$  and  $\hat{\mathcal{B}}$ , we have the identity*

$$m_{\text{H}}^{\mathcal{B}}(\mathcal{A}_1, \mathcal{A}_2) = m_{\text{H}}^{\hat{\mathcal{B}}}(\mathcal{A}_1, \mathcal{A}_2).$$

For the sake of simplicity, if the compact subset of the metric space including all subspaces of interest is fixed, we denote the Hausdorff metric introduced in (2.1) as  $m_H(\cdot, \cdot)$ . Finally, if  $\{\mathcal{A}_n\}_{n=1}^\infty$  and  $\mathcal{A}$  are open subsets of  $\mathcal{B}$ , we say that the sequence  $\{\mathcal{A}_n\}_{n=1}^\infty$  converges in the sense of Hausdorff towards  $\mathcal{A}$  if

$$\lim_{n \rightarrow \infty} m_H(\mathcal{A}_n, \mathcal{A}) = 0$$

and we denote such convergence as  $\mathcal{A}_n \xrightarrow{H} \mathcal{A}$ .

The shape functional  $\Omega \mapsto \sup_{\mathbf{g} \in \mathcal{G}} H(\mathbf{u}_{\Omega, \mathbf{g}}, \Omega)$  is not continuous if  $\mathcal{S}_{\text{adm}}$  is a generic class of open domains in  $\mathbb{R}^d$ , since it relies on the computation of  $\mathbf{u}_\Omega$ . Therefore, one restricts the class of admissible domains to domains satisfying the  $\varepsilon$ -cone condition see [31, Definition 2.4.1].

**DEFINITION 2.4** ( $\varepsilon$ -cone condition). *Let  $\varepsilon$  be a positive parameter. For any  $\mathbf{x} \in \mathbb{R}^d$  and any unit vector  $\boldsymbol{\xi} \in \mathbb{R}^d$ , we denote  $B_\varepsilon(\mathbf{x})$  the ball of radius  $\varepsilon$  centered in  $\mathbf{x}$ , and  $C_\varepsilon(\mathbf{x}, \boldsymbol{\xi})$  the open cone of vertex  $\mathbf{x}$  (without its vertex), of direction  $\boldsymbol{\xi}$  defined as*

$$C_\varepsilon(\mathbf{x}, \boldsymbol{\xi}) = \{\mathbf{y} \in \mathbb{R}^d : \langle \mathbf{y} - \mathbf{x}, \boldsymbol{\xi} \rangle_{\mathbb{R}^d} \geq \cos(\varepsilon) |\mathbf{y} - \mathbf{x}| \text{ and } 0 < |\mathbf{y} - \mathbf{x}| < \varepsilon\}.$$

An open set  $\mathcal{A}$  is said to satisfy the  $\varepsilon$ -cone condition if, for all  $\mathbf{x}$  on the boundary of  $\mathcal{A}$ , there exists a unit vector  $\boldsymbol{\xi}$  such that for any  $\mathbf{y} \in B_\varepsilon(\mathbf{x})$ , the cone  $C_\varepsilon(\mathbf{y}, \boldsymbol{\xi})$  is contained in  $\mathcal{A}$ . We denote  $\mathcal{D}_\varepsilon(\mathbb{R}^d)$  the set of all open domains in  $\mathbb{R}^d$  fulfilling the  $\varepsilon$ -cone condition. For any compact set  $\mathcal{B} \subset \mathbb{R}^d$ , we denote  $\mathcal{D}_\varepsilon(\mathcal{B})$  the subset of all open domains in  $\mathcal{D}_\varepsilon(\mathbb{R}^d)$  contained into  $\mathcal{B}$ :

$$(2.2) \quad \mathcal{D}_\varepsilon(\mathcal{B}) = \{\mathcal{A} \subset \mathcal{B} : \mathcal{A} \text{ open, and satisfying the } \varepsilon\text{-cone condition}\}.$$

The continuity of  $\Omega \in \mathcal{S}_{\text{adm}} \mapsto \sup_{\mathbf{g} \in \mathcal{G}} H(\mathbf{u}_{\Omega, \mathbf{g}}, \Omega) \in \mathbb{R}$  relies on the following result, proven in [15] and reported in [31, Theorem 3.2.13].

**THEOREM 2.5.** *We consider  $\varepsilon > 0$ , and  $\mathcal{B} \subset \mathbb{R}^d$  to be a compact set. Let  $\{\Omega_n\}_{n=1}^\infty$  and  $\Omega$  be open domains in  $\mathcal{S}_{\text{adm}} \subset \mathcal{D}_\varepsilon(\mathcal{B})$ , and let  $\Omega_n \xrightarrow{H} \Omega$ . Then, the sequence  $\{\mathbf{u}_{\Omega_n}\}_{n=1}^\infty$  converges towards  $\mathbf{u}_\Omega$ , where  $\mathbf{u}_\Omega$  is the solution of the linear elasticity problem on  $\Omega$  and  $\mathbf{u}_{\Omega_n}$  is the solution on  $\Omega_n$  for all  $n \geq 0$ .*

**Theorem 2.5** combined with the structure of the constraint stated in (1.3) ensures that the shape functional  $\Omega \mapsto \sup_{\mathbf{g} \in \mathcal{G}} H(\mathbf{u}_{\Omega, \mathbf{g}}, \Omega)$  is continuous on a class of uniformly bounded open sets satisfying the  $\varepsilon$ -cone condition for some positive  $\varepsilon$ .

**2.2. Theoretical results.** From now on, we consider that all admissible domains satisfy the  $\varepsilon$ -cone condition, that they are uniformly bounded by a compact set  $\mathcal{B}$ , and that  $\mathcal{S}_{\text{adm}}$  is a closed subset of  $\mathcal{D}_\varepsilon(\mathcal{B})$  for some  $\varepsilon > 0$ . We suppose that the set of admissible loads is bounded, convex and finite-dimensional, and the mapping  $\mathbf{g} \mapsto H(\mathbf{u}_{\Omega, \mathbf{g}}, \Omega)$  is a convex function. The objective of this section is to justify the approach of the engineers and provide some results on the convergence of the solution when the number of loading conditions  $N$  increases.

We state all the results of this section for the following generic optimization problem, where the dependence from the state is kept implicit

$$(2.3) \quad \left| \begin{array}{l} \text{Find the admissible shape } \Omega \in \mathcal{S}_{\text{adm}} \text{ minimizing the volume } \text{Vol}(\Omega) \\ \text{under the constraint } \sup_{\mathbf{g} \in \mathcal{G}} h(\mathbf{g}, \Omega) \leq \tau. \end{array} \right.$$

We suppose that  $\mathcal{G}$  is a compact convex set contained in a finite dimensional space  $(\mathcal{Y}, \|\cdot\|_{\mathcal{Y}})$ , and that  $h : \mathcal{G} \times \mathcal{S}_{\text{adm}} \rightarrow \mathbb{R}$  is a real-valued function. The mapping  $\Omega \mapsto h(\mathbf{g}, \Omega)$  can be seen as an instance of a family of shape functions depending on the parameter  $\mathcal{G}$ . Moreover, we assume that the functions satisfy the following conditions:

- (i) the mapping  $\mathbf{g} \mapsto h(\mathbf{g}, \Omega)$  is convex and bounded for all admissible  $\Omega \in \mathcal{S}_{\text{adm}}$ ;
- (ii) for all choice of the parameter  $\mathbf{g} \in \mathcal{G}$ , the mapping  $\Omega \mapsto h(\mathbf{g}, \Omega)$  is shape differentiable.

A first result on the solution of problem (1.2) is provided by the following proposition, which applies to the case where the set of admissible loads is polyhedral.

**PROPOSITION 2.6.** *Let  $\mathcal{G}$  be a compact convex polyhedral subset of the Banach space  $\mathcal{Y}$  with  $N$  vertices  $\mathbf{g}_1, \dots, \mathbf{g}_N$ , and  $h : \mathcal{G} \times \mathcal{S}_{\text{adm}} \rightarrow \mathbb{R}$  a real-valued function satisfying the assumptions (i) - (ii) stated above. Then, the solution of problem (2.3) is equivalent to the solution of the following constrained optimization problem:*

$$(2.4) \quad \left| \begin{array}{l} \text{Find the admissible shape } \Omega \in \mathcal{S}_{\text{adm}} \text{ minimizing the volume } \text{Vol}(\Omega) \\ \text{under the } N \text{ inequality constraints: } \forall i \in \{1, \dots, N\}, h(\mathbf{g}_i, \Omega) \leq \tau. \end{array} \right.$$

**Proposition 2.6** follows directly from the application of **Proposition 2.1** to the inequality constraint. Moreover, the formulation of **Proposition 2.1** as an optimization problem with multiple constraints makes it conforming with the *nullspace optimization algorithm* introduced in [27, 26] which simplifies the numerical implementation.

Having proven a result on the solution of problem (2.3) for convex polyhedra, we aim to extend it to more general compact convex sets. Let  $\mathcal{G}$  be a compact and convex subset of a Banach space  $\mathcal{Y}$ , and  $\{\mathcal{G}_n\}_{n=1}^{\infty}$  a sequence of convex compact polyhedral subsets of  $\mathcal{Y}$  converging towards  $\mathcal{G}$  with respect to the Hausdorff distance. The next step is the evaluation of the convergence of the minimizers of a sequence of problems in the form (2.3). A first important remark concerns the relation of the admissible sets in two different problems, when the corresponding sets of parameters are nested one into the other.

**LEMMA 2.7.** *Let us consider two subsets  $\mathcal{G}_1, \mathcal{G}_2$  of a Banach space  $\mathcal{Y}$  such that  $\mathcal{G}_1 \subset \mathcal{G}_2$ . We denote  $E_1, E_2$  the subsets of  $\mathcal{S}_{\text{adm}} \subset \mathcal{D}_{\varepsilon}(\mathcal{B})$  where the inequality constraint of problem (2.3) is satisfied for the sets of parameters  $\mathcal{G}_1$  and  $\mathcal{G}_2$  respectively:*

$$E_i = \left\{ \Omega \in \mathcal{S}_{\text{adm}} : \sup_{\mathbf{g} \in \mathcal{G}_i} h(\mathbf{g}, \Omega) \leq \tau \right\}, \quad \text{for } i \in \{1, 2\}.$$

Then,  $E_2 \subset E_1$ .

*Proof.* Let us consider  $\Omega \in E_2$ . Since all  $\mathbf{g}_1 \in \mathcal{G}_1$  belongs also to  $\mathcal{G}_2$ , we have that  $h(\mathbf{g}_1, \Omega) \leq \tau$  for all  $\mathbf{g}_1 \in \mathcal{G}_1$ . Thus  $\Omega \in E_1$ .  $\square$

Thanks to **Lemma 2.7**, we can prove the following result about the convergence of the solutions of a sequence of problems in the form (2.3).

**PROPOSITION 2.8.** *We consider  $\{\mathcal{G}_n\}_{n=1}^{\infty}$  to be an increasing sequence of compact subsets of  $\mathcal{Y}$  where  $\mathcal{G}_i \subset \mathcal{G}_j$  if  $i < j$  and such that  $\mathcal{G} = \overline{\bigcup_{i=1}^{\infty} \mathcal{G}_i}$  is compact as well. Let  $h : \mathcal{G} \times \mathcal{S}_{\text{adm}} \rightarrow \mathbb{R}$  be a function that satisfies the assumptions (i) and (ii),  $\mathcal{S}_{\text{adm}} \subset \mathcal{D}_{\varepsilon}(\mathcal{B})$  closed, and  $\tau \in \mathbb{R}$  be a given threshold. As in **Lemma 2.7**, we denote  $E_i$  the subset of admissible domains  $\mathcal{S}_{\text{adm}}$  such that, if  $\Omega \in E_i$ , then  $h(\mathbf{g}, \Omega) \leq \tau$  for*

all  $g \in \mathcal{G}_i$ . Finally, we denote  $E$  the set of admissible domains such defined as

$$E = \left\{ \Omega \in \mathcal{S}_{\text{adm}} : \sup_{\mathbf{g} \in \mathcal{G}} h(\mathbf{g}, \Omega) \leq \tau \right\},$$

and we suppose that neither any set  $E_i$ , nor the set  $E$  is empty. Then, the sequence  $\{E_i\}_{i=1}^{\infty}$  is decreasing, in the sense that  $E_i \supseteq E_j$  if  $i < j$ ,  $E = \bigcap_{i=1}^{\infty} E_i$ , and  $E$  as well as all  $E_i$  are closed subsets of  $\mathcal{S}_{\text{adm}}$  with respect to its metric  $m_{\mathbb{H}}$ .

*Proof.* The fact that  $\{E_i\}_{i=1}^{\infty}$  is a decreasing sequence follows from [Lemma 2.7](#). Next, we prove the identity  $E = \bigcap_{i=1}^{\infty} E_i$ . The inclusion  $E \subset \bigcap_{i=1}^{\infty} E_i$  is, again, a direct consequence of [Lemma 2.7](#) since, for all  $i > 0$ , we suppose that  $\mathcal{G} \supseteq \mathcal{G}_i$ . In order to prove the converse inclusion we suppose that  $\Omega \in E_i$  for all  $i > 0$ . Since we defined the set  $\mathcal{G}$  as  $\mathcal{G} = \bigcup_{i=1}^{\infty} \mathcal{G}_i$ , for all  $\mathbf{g} \in \mathcal{G}$ , there exists a sequence  $\{\mathbf{g}_i\}_{i=1}^{\infty}$  such that  $\mathbf{g}_i \in \mathcal{G}_i$  for all  $i > 0$ , and  $\mathbf{g}_i \rightarrow \mathbf{g}$ . By hypothesis,  $\mathbf{g} \mapsto h(\mathbf{g}, \Omega)$  is convex on the finite-dimensional space  $\mathcal{Y}$  and it is bounded. Thus, such mapping is also continuous (see [\[36, Corollary 10.1.1\]](#)). By the definition of the sets  $\{E_i\}_{i=1}^{\infty}$  and the sequence  $\{\mathbf{g}_i\}_{i=1}^{\infty}$ , and by the continuity of  $\mathbf{g} \mapsto h(\mathbf{g}, \Omega)$ , we deduce that  $h(\mathbf{g}, \Omega) \leq \tau$ , and we conclude that  $\Omega \in E$ .

Let  $i \in \mathbb{N}$ . In order to prove that  $E_i$  is a closed set, we consider the function  $\Phi_i : \mathcal{S}_{\text{adm}} \rightarrow \mathbb{R}^+$ , mapping  $\Omega \mapsto \sup_{\mathbf{g} \in \mathcal{G}_i} h(\mathbf{g}, \Omega)$ . Such function is well-defined and continuous on  $\mathcal{S}_{\text{adm}}$ , since the set of parameters  $\mathcal{G}_i$  is compact. Thus, we deduce that  $E_i = \Phi_i^{-1}([0, M])$  is a closed subset of  $\mathcal{S}_{\text{adm}}$ . Since  $E = \bigcap_{i=1}^{\infty} E_i$ , we conclude that  $E$  is closed with respect to the Hausdorff metric in  $\mathcal{S}_{\text{adm}}$  as well.  $\square$

Now, we can state the main result of this section, which is about the convergence of the solution of a sequence of shape optimization problems in the form [\(2.6\)](#) with an increasingly accurate approximation of the set  $\mathcal{G}$ .

**THEOREM 2.9.** *We consider a compact set  $\mathcal{B} \subset \mathbb{R}^d$ , and a family of open domains  $\mathcal{S}_{\text{adm}}$ , uniformly bounded by  $\mathcal{B}$  and closed in  $\mathcal{D}_{\varepsilon}(\mathcal{B})$ . Let  $h : \mathcal{G} \times \mathcal{S}_{\text{adm}} \rightarrow \mathbb{R}$  be a function fulfilling assumptions (i) and (ii),  $\tau \in \mathbb{R}$  a given threshold, and  $\{\mathcal{G}_n\}_{n=1}^{\infty}$  a sequence of compact subsets of  $\mathcal{Y}$  satisfying the hypotheses of [Proposition 2.8](#). Let  $\{\Omega_i\}_{i=1}^{\infty}$  be a sequence of domains such that  $\Omega_i \in \arg \min_{\Omega \in E_i} \text{Vol}(\Omega)$  for all  $i \in \mathbb{N}$ . Then,  $\{\Omega_i\}_{i=1}^{\infty}$  admits a converging sub-sequence with respect to the Hausdorff metric, and any  $\Omega_{\infty}$  in the limit class is a solution of problem [\(2.3\)](#).*

*Proof.* Let us consider a sequence  $\{\Omega_i\}_{i=1}^{\infty}$  such that  $\Omega_i \in E_i$  for all  $n > 0$ . All sets  $E_i$  are closed subset of  $\mathcal{S}_{\text{adm}} \subset \mathcal{D}_{\varepsilon}(\mathcal{B})$  embedded into one another, and  $\mathcal{D}_{\varepsilon}(\mathcal{B})$  is sequentially compact with respect to the Hausdorff metric [\[31, Theorem 2.4.10\]](#). Thus,  $\{\Omega_i\}_{i=1}^{\infty}$  admits a sub-sequence converging towards  $\Omega_{\infty} \in \mathcal{D}_{\varepsilon}(\mathcal{B})$ , and  $\Omega_{\infty} \in E_i$  for all  $i \in \mathbb{N}$ . Thanks to [Proposition 2.8](#) we deduce that  $\Omega_{\infty} \in E$ .

Finally, in order to prove that  $\Omega_{\infty} \in \arg \min_{\Omega \in E} \text{Vol}(\Omega)$ , we reason by contradiction. Let  $\varepsilon > 0$  and  $\Omega_{\varepsilon} \in E$  such that  $\text{Vol}(\Omega_{\infty}) = \text{Vol}(\Omega_{\varepsilon}) + \varepsilon$ . Since  $\text{Vol}(\cdot)$  is a continuous function with respect to the metric  $m_{\mathbb{H}}$ , there exists  $N_{\varepsilon} > 0$  such that, for all  $n > N_{\varepsilon}$ ,  $\text{Vol}(\Omega_n) > \text{Vol}(\Omega_{\varepsilon}) + \varepsilon/2$ . This result is in contradiction with the assumption  $\Omega_n \in \arg \min_{\Omega \in E_n} \text{Vol}(\Omega)$ , since  $\Omega_{\varepsilon} \in E \subset E_n$ . Therefore, we conclude that  $\Omega_{\infty} \in \arg \min_{\Omega \in E} \text{Vol}(\Omega)$ .  $\square$

One technique to solve problem [\(2.3\)](#) for a constraint functional  $h(\cdot, \cdot)$  satisfying conditions (i) and (ii) consists in solving an approximate problem where the set of admissible parameters  $\mathcal{G}$  is replaced by a convex polyhedral set  $\mathcal{G}_N$  with  $N$  vertices. [Theorem 2.9](#) suggests that, by increasing the accuracy of the approximation of  $\mathcal{G}$  by  $\mathcal{G}_N$ , the solution of the approximate problem converges towards the solution of

the original one. The approximate problems can then be solved as simple constrained optimization problem using [Proposition 2.6](#).

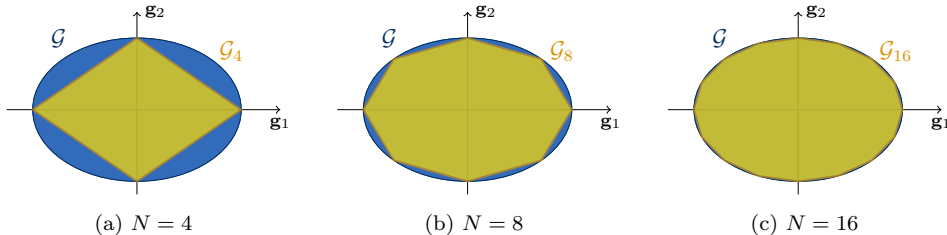


FIG. 1. Approximation of the set of admissible parameters by convex polyhedra with an increasing number of vertices  $N$ .

This approach suffers from two notable drawbacks.

- The first one is the fact that none of the polyhedral sets considered by [Proposition 2.6](#) is a conservative approximation of the original set of admissible parameters  $\mathbf{g}$ . Therefore, for any approximation  $\mathcal{G}_N$  of  $\mathcal{G}$ , denoting  $\Omega_N$  the solution of the corresponding optimization problem, there exists a parameter  $\tilde{\mathbf{g}} \in (\mathcal{G} \setminus \mathcal{G}_N) \neq \emptyset$  such that  $h(\tilde{\mathbf{g}}, \Omega_N) > \tau$ . A possible solution to this issue consists in considering a sequence of polyhedral sets converging towards  $\mathcal{G}^*$  strictly containing  $\mathcal{G}$ . However, the convergence of the solutions of the approximated problems towards the solution of the original would be lost.
- A second important issue from the numerical point of view concerns the number of points that are necessary to accurately approximate the finite-dimensional set  $\mathcal{G}$ . Indeed, as shown in [9], given a convex set  $\mathcal{G} \subset \mathbb{R}^n$  of class  $\mathcal{C}^2$  and a tolerance  $\epsilon > 0$ , the minimal number of vertices  $N_{\mathcal{G},\epsilon}$  such that the Hausdorff distance between their convex hull and  $\mathcal{G}$  is bounded by

$$(2.5) \quad N_{\mathcal{G},\epsilon} \geq \left( \frac{c(\mathcal{G})}{\epsilon} \right)^{\frac{n-1}{2}},$$

where  $c(\mathcal{G})$  is a constant depending on the shape of the convex set. [Equation \(2.5\)](#) proves that the number of vertices that are necessary to approximate a given convex set for a given precision increases exponentially with respect to the dimension of the space of parameters. Since any vertex in the approximating polyhedron corresponds to a constraint in problem (2.3), an exponentially increasing number of constraints has to be evaluated for the solution of the optimization problem, indicating that this approach suffers from the curse of dimensionality.

**3. An approach based on subdifferentials.** Another approach to solve problem (1.2) by a gradient-based method consists in differentiating directly the constraint function  $\Omega \mapsto \sup_{\mathbf{g} \in \mathcal{G}} H(\mathbf{u}_\Omega, \mathbf{g}, \Omega)$ . The question of the derivative with respect to the domain of non-differentiable shape functionals has been considered in literature from different points of view. The authors of [34, 1] are interested in the optimization with respect to non-smooth functionals. In [4, 20, 13, 12], the quantity of interest consists in the first eigenvalue of different functionals, which can be expressed as minima of suitable Rayleigh quotients. In particular, the approach proposed in [13, 12] consists in the computation of a semi-derivative in the sense of Danskin [23] by applying a

result from Delfour and Zolésio [25, Theorem 2.1, Chapter 10] on the sensitivity of a minimum with respect to a parameter. In this section we present an approach inspired by the methods of [30], which relies on the notion of subdifferentiability of non-smooth functions as introduced by Clarke in [17].

**3.1. Introduction to Clarke’s subdifferential.** At first, we recall the definitions of generalized directional derivative, strict differentiability, and subdifferential in the sense of Clarke, as found in [17, Section 2.1].

DEFINITION 3.1 (Generalized directional derivative). *Let  $\mathcal{X}$  be a Banach space,  $x, v \in \mathcal{X}$ , and  $f : \mathcal{X} \rightarrow \mathbb{R}$  a function which is Lipschitz continuous in a neighborhood of  $x$ . The generalized directional derivative of  $f$  in  $x$  in the direction  $v$  is defined as*

$$f^\circ(x; v) = \lim_{\substack{y \rightarrow x \\ t \searrow 0^+}} \frac{f(y + tv) - f(y)}{t}.$$

DEFINITION 3.2 (Strictly differentiable function). *Let us denote  $\mathcal{X}^*$  the topological dual of the Banach space  $\mathcal{X}$ . A real-valued function  $f$  defined on  $\mathcal{X}$  is strictly differentiable in  $x \in \mathcal{X}$  if it admits a generalized directional derivative  $f^\circ(x; v)$  for all  $v \in \mathcal{X}$ , and there exists a linear functional  $D_x^s \in \mathcal{X}^*$  such that, for all  $v \in \mathcal{X}$ ,*

$$f^\circ(x; v) = D_x^s(v).$$

Next, we present the notion of subdifferential in the sense of Clarke, introduced in [17] as “generalized gradient” and extending the results of Danskin [23].

DEFINITION 3.3 (subdifferential in the sense of Clarke). *Let  $f : \mathcal{X} \rightarrow \mathbb{R}$  be a function defined on the Banach space  $\mathcal{X}$ , which is Lipschitz continuous in a neighborhood of  $x \in \mathcal{X}$ . The subdifferential in the sense of Clarke of  $f$  in  $x$  is the subset of  $\mathcal{X}^*$  defined as*

$$\partial f(x) = \{L \in \mathcal{X}^* : f^\circ(x; v) \geq L(v) \text{ for all } v \in \mathcal{X}\}.$$

We state now a result presented as [17, Corollary 2 of Theorem 2.8.2] and referred in [30, Section 4.2].

PROPOSITION 3.4. *Let  $\mathcal{X}$  be a Banach space,  $\mathcal{T}$  a metrisable, sequentially compact topological space,  $x \in \mathcal{X}$ , and  $\{f(\cdot, t)\}_{t \in \mathcal{T}}$  a family of functions such that:*

- (A1)  *$y \mapsto f(y, t)$  is Lipschitz continuous for all  $y$  in a neighborhood  $U_x$  of  $x$  and for all  $t \in \mathcal{T}$ ;*
- (A2) *for any  $y \in U_x$  the mapping  $t \mapsto f(y, t)$  is upper-semicontinuous;*
- (A3) *the set  $\{f(x, t) : t \in \mathcal{T}\} \subset \mathbb{R}$  is bounded;*
- (A4)  *$f(\cdot, t)$  is strictly differentiable in  $U_x$ , and the strict derivative  $D_y^s f(y, t)$  is continuous in  $U_x \times \mathcal{T}$ .*

We denote  $F : \mathcal{X} \rightarrow \mathbb{R}$  the function mapping  $y \mapsto F(y) = \sup_{t \in \mathcal{T}} f(y, t)$ , which is defined, finite, and Lipschitz continuous in  $U_x$ . Moreover, we denote  $\mathcal{T}(y) = \{t \in \mathcal{T} : f(y, t) = F(y)\}$  the subset of the set of the parameters  $\mathcal{T}$  where the maximum in the definition of  $F(\cdot)$  is attained, and we remark that  $\mathcal{T}(y)$  is not empty for all  $y \in U_x$ .

Then, the subdifferential in the sense of Clarke of  $F$  exists for all  $y \in U_x$  and is given by:

$$(3.1) \quad \partial F(y) = \left\{ \int_{\mathcal{T}} D_y^s f(y, t) \, d\mu(t) : \mu \in P[\mathcal{T}(y)] \right\},$$

where the notation  $P[\mathcal{S}]$  denotes the collection of probability Radon measures on a measurable subset  $\mathcal{S}$  of  $\mathcal{T}$ .

*Remark 3.5.* In [17, Section 2.2] is recalled that any continuously differentiable function in  $x \in \mathcal{X}$  is also strictly differentiable in  $x$ . Thus, in [Proposition 3.4](#) we can suppose that  $f(\cdot, t)$  is differentiable in  $U_x$  and the derivative  $\frac{\partial f}{\partial y}(y, t)$  is continuous on  $U_x \times \mathcal{T}$ , and the proposition still holds true.

Let  $f : \mathcal{X} \times \mathcal{T} \rightarrow \mathbb{R}$  satisfy the hypotheses of [Proposition 3.4](#), and  $F : \mathcal{X} \rightarrow \mathbb{R}$  be the mapping  $x \mapsto \max_{t \in \mathcal{T}} f(x, t)$ . Finally, let us consider  $y \in \mathcal{X}$ , and  $\bar{t} \in \mathcal{T}(y)$  a parameter for which  $f(x, t) = F(x)$ . Since  $P[\mathcal{T}(y)]$  contains the Dirac measure concentrated in  $\bar{t}$ , the derivative  $\frac{\partial f}{\partial y}(y, \bar{t}) \in \mathcal{X}^*$  belongs to the subdifferential  $\partial F(y)$ . Moreover, if  $F$  is differentiable in  $y \in \mathcal{X}$ , the subdifferential reduces to a singleton.

**3.2. Application to shape optimization problems.** Similarly to what has been done in [subsection 2.2](#), we consider a generic optimization problem without an explicit expression of the state like problem (2.3). For the sake of simplicity, we denote  $\Phi : \mathcal{S}_{\text{adm}} \rightarrow \mathbb{R}$  the shape functional defined as

$$(3.2) \quad \Phi(\Omega) = \sup_{\mathbf{g} \in \mathcal{G}} h(\mathbf{g}, \Omega).$$

Unfortunately, [Proposition 3.4](#) cannot apply directly to differentiate  $\Phi$ , since the space  $\mathcal{S}_{\text{adm}}$  provided with the Hausdorff metric  $m_{\text{H}}$  defined in (2.1) is not a Banach space. Such issue can be bypassed thanks to the definition of the shape derivative according to Hadamard. Indeed, for a given admissible domain  $\Omega \in \mathcal{S}_{\text{adm}}$ , the deformation field  $\boldsymbol{\theta}$  at the core of Hadamard's moving boundaries approach belongs to the Banach space  $W^{1,\infty}(\mathbb{R}^d)^d$ . With this in mind, we can extend the concepts of subdifferential to shape functionals.

**DEFINITION 3.6** (Subdifferential of a shape functional). *Let  $\Omega \in \mathcal{S}_{\text{adm}}$  be a domain in  $\mathbb{R}^d$ , and  $J : \mathcal{S}_{\text{adm}} \rightarrow \mathbb{R}$  a shape functional such that the mapping  $\boldsymbol{\theta} \mapsto J(\Omega_{\boldsymbol{\theta}})$  admits a Gâteaux derivative  $dJ(\Omega; \boldsymbol{\theta})$  for all  $\boldsymbol{\theta} \in W^{1,\infty}(\mathbb{R}^d)^d$ . Then, the subdifferential of  $J$  in  $\Omega$  is defined as*

$$\partial J(\Omega) = \left\{ L \in \left( W^{1,\infty}(\mathbb{R}^d)^d \right)^* : dJ(\Omega; \boldsymbol{\theta}) \geq L(\boldsymbol{\theta}) \text{ for all } \boldsymbol{\theta} \in W^{1,\infty}(\mathbb{R}^d)^d \right\}.$$

We can now state a result for shape functionals analogous to [Proposition 3.4](#).

**PROPOSITION 3.7.** *Let  $\mathcal{S}_{\text{adm}}$  be a family of uniformly bounded open domains in  $\mathbb{R}^d$  endowed with the topology induced by the Hausdorff metric  $m_{\text{H}}$ , and  $\mathcal{G}$  a compact subset of a Banach space  $(\mathcal{Y}, \|\cdot\|)$ . Let  $\Omega \in \mathcal{S}_{\text{adm}}$  be an admissible domain, and  $h : \mathcal{G} \times \mathcal{S}_{\text{adm}} \rightarrow \mathbb{R}$  a shape functional such that:*

- (SA1)  $\tilde{\Omega} \mapsto h(\mathbf{g}, \tilde{\Omega})$  is Lipschitz continuous in a neighborhood  $U_{\Omega}$  of  $\Omega$  for any choice of the parameter  $\mathbf{g} \in \mathcal{G}$ ;
- (SA2)  $\mathbf{g} \mapsto h(\mathbf{g}, \tilde{\Omega})$  is convex and bounded for all  $\tilde{\Omega} \in U_{\Omega}$ ;
- (SA3)  $\tilde{\Omega} \mapsto h(\mathbf{g}, \tilde{\Omega})$  is Fréchet differentiable in  $U_{\Omega}$  for any  $\mathbf{g} \in \mathcal{G}$ ;
- (SA4) the Fréchet derivative  $\frac{\partial h}{\partial \tilde{\Omega}}(\mathbf{g}, \tilde{\Omega}) \in \left( W^{1,\infty}(\mathbb{R}^d)^d \right)^*$  is continuous in  $\mathcal{G} \times U_{\Omega}$ .

We denote  $\Phi : \mathcal{S}_{\text{adm}} \rightarrow \mathbb{R}$  the shape functional

$$\Omega \mapsto \Phi(\Omega) = \max_{\mathbf{g} \in \mathcal{G}} h(\mathbf{g}, \Omega),$$

where the maximum is attained thanks to the convexity of  $h(\cdot, \mathbf{g})$  and compactness of  $\mathcal{G}$ . Then, the functional  $\Phi(\cdot)$  admits a subdifferential  $\partial\Phi(\Omega)$  in  $\Omega$ , and its expression is given by

$$\partial\Phi(\Omega) = \left\{ \int_{\mathcal{G}} \frac{\partial h}{\partial \Omega}(\mathbf{g}, \Omega) d\mu(\mathbf{g}) : \mu \in P[\mathcal{G}(\Omega)] \right\} \subset \left( W^{1,\infty}(\mathbb{R}^d)^d \right)^*.$$

*Proof.* We consider the class  $\Theta_\Omega \subset W^{1,\infty}(\mathbb{R}^d)^d$  of admissible deformations defined as

$$\Theta_\Omega = \left\{ \boldsymbol{\theta} \in W^{1,\infty}(\mathbb{R}^d)^d : \Omega_{\boldsymbol{\theta}} \in U_\Omega \right\}.$$

We introduce the function  $f_\Omega : \mathcal{G} \times \Theta_\Omega \rightarrow \mathbb{R}$  mapping  $(\mathbf{g}, \boldsymbol{\theta}) \mapsto f_\Omega(\mathbf{g}, \boldsymbol{\theta}) = h(\mathbf{g}, \Omega_{\boldsymbol{\theta}})$ . In order to prove [Proposition 3.7](#), we verify that  $f_\Omega$  satisfies all the hypotheses of [Proposition 3.4](#). At first, we observe that the set  $\mathcal{G}$  is compatible with the hypotheses of [Proposition 3.4](#), since it is a compact subset of the Banach space  $\mathcal{Y}$  with respect to the Hausdorff metric  $m_H$ . The set  $\Theta_\Omega$  is a neighborhood of the origin in the Banach space  $W^{1,\infty}(\mathbb{R}^d)^d$ .

The conditions (A1) to (A4) of [Proposition 3.4](#) are satisfied by  $f_\Omega$  thanks to assumptions (SA1) and (SA2). In particular, the continuity of  $f_\Omega(\cdot, \boldsymbol{\theta})$  for all  $\boldsymbol{\theta} \in \Theta_\Omega$  is ensured by the convexity of  $\mathbf{g} \mapsto h(\mathbf{g}, \tilde{\Omega})$  for all  $\tilde{\Omega} \in U_\Omega$ . The existence and continuity of the strict derivative of  $\boldsymbol{\theta} \mapsto f_\Omega(\mathbf{g}, \boldsymbol{\theta})$  follow from assumptions (SA3) and (SA4) and from [Remark 3.5](#). Therefore, the function  $\boldsymbol{\theta} \mapsto F_\Omega(\boldsymbol{\theta}) = \max_{\mathbf{g} \in \mathcal{G}} f_\Omega(\mathbf{g}, \boldsymbol{\theta})$  is well defined, and it admits a subdifferential  $\partial F_\Omega(\boldsymbol{\theta})$  with the following expression

$$\partial F_\Omega(\boldsymbol{\theta}) = \left\{ \int_{\mathcal{G}} \frac{\partial f_\Omega}{\partial \boldsymbol{\theta}}(\mathbf{g}, \boldsymbol{\theta}) d\mu(\mathbf{g}) : \mu \in P[\mathcal{G}(\Omega)] \right\} \subset \left( W^{1,\infty}(\mathbb{R}^d)^d \right)^*.$$

Thanks to the definitions of the functionals  $\Phi$  and  $F_\Omega$  we have that, for all  $\boldsymbol{\theta} \in \Theta_\Omega$ ,  $\Phi(\Omega_{\boldsymbol{\theta}}) = F_\Omega(\boldsymbol{\theta})$  and, in particular,  $\Phi(\Omega) = F_\Omega(\mathbf{0})$ . Thus,  $\partial\Phi(\Omega) = \partial F_\Omega(\mathbf{0})$ .  $\square$

[Proposition 3.7](#) provides a method to compute elements of the subdifferential according to the shape  $\partial\Phi(\Omega)$  by computing a value of the parameter  $\mathbf{g} \in \mathcal{G}$  where  $h(\Omega, \mathbf{g})$  attains its maximum. Differently from the case studied in [section 2](#), the convexity of the set  $\mathcal{G}$  of external loads is not required. It should also be remarked that any element of the subdifferential defines a direction of descent for the functional  $\Phi$ , albeit not necessarily optimal if  $\partial\Phi(\Omega)$  is not a singleton.

**3.3. Algorithmic implementation.** Let us consider the same notations of [Proposition 3.7](#):  $\mathcal{G}$  is a compact subset of a Banach space  $(\mathcal{Y}, \|\cdot\|)$ ,  $h : \mathcal{G} \times \mathcal{S}_{\text{adm}} \rightarrow \mathbb{R}$  a function satisfying the conditions (SA1) - (SA4) of [Proposition 3.7](#), and  $\Phi(\cdot)$  the shape functional mapping  $\Omega \mapsto \max_{\mathbf{g} \in \mathcal{G}} h(\mathbf{g}, \Omega)$ .

In [subsection 3.2](#) we provided the theoretical framework for the computation of the subdifferential of  $\Phi(\cdot)$ . Here we provide a procedure to compute one element to the subdifferential  $\partial\Phi(\Omega)$ . The procedure can be divided in two steps. First, we identify a parameter  $\bar{\mathbf{g}} \in \arg \max_{\mathbf{g} \in \mathcal{G}} h(\mathbf{g}, \Omega) \subset \mathcal{G}$  for which the maximum of  $h(\cdot, \Omega)$  is attained. The maximum is attained in at least one point, since  $\mathcal{G}$  is compact, and  $h(\cdot, \Omega)$  is convex and bounded (see [Proposition 2.1](#)). Next, the shape derivative of the term  $h(\bar{\mathbf{g}}, \Omega)$  is computed using the classical methods of boundary variation. [Proposition 3.7](#) ensures that the shape derivative of  $h(\bar{\mathbf{g}}, \Omega)$  belongs to the subdifferential  $\partial\Phi(\Omega)$ .

Different possible methods can be considered to identify the parameter  $\bar{\mathbf{g}}$  depending on the nature of the set  $\mathcal{G}$  and the function  $h(\cdot, \Omega)$ . If the mapping  $\mathbf{g} \mapsto h(\mathbf{g}, \Omega)$  is differentiable with respect to  $\mathbf{g}$  and  $\mathcal{G}$  is a subset of a Hilbert space, a simple gradient-descent method can be implemented to identify  $\bar{\mathbf{g}}$ . If further hypotheses apply on the constraint functional or on the set of admissible parameters, *ad hoc* methods can be used. An example for the case where  $\mathbf{g} \mapsto h(\mathbf{g}, \Omega)$  is a quadratic function and  $\mathcal{G}$  an ellipsoid is provided in [subsection 4.1](#).

#### 4. Numerical results.

**4.1. 3D Cantilever.** As first numerical application, we consider the optimization of a 3D cantilever structure under a constraint on the mechanical compliance given by

$$\mathcal{C}(\mathbf{u}_{\Omega, \mathbf{g}}, \Omega) = \int_{\Omega} \mathbf{f} \cdot \mathbf{u}_{\Omega, \mathbf{g}} \, d\mathbf{x} + \int_{\Gamma_N} \mathbf{g} \cdot \mathbf{u}_{\Omega, \mathbf{g}} \, ds.$$

Then we consider the following problem

$$(4.1) \quad \left\{ \begin{array}{l} \text{Find the admissible shape } \Omega \in \mathcal{S}_{\text{adm}} \text{ minimizing the volume } \text{Vol}(\Omega) \\ \text{under the constraint } \sup_{\mathbf{g} \in \mathcal{G}} \mathcal{C}(\mathbf{u}_{\Omega, \mathbf{g}}, \Omega) \leq \tau, \\ \text{where the displacement } \mathbf{u}_{\Omega, \mathbf{g}} \in H_{\Gamma_D}^1(\Omega)^d \text{ solves (1.1).} \end{array} \right.$$

The initial condition of the structure is presented in [Figure 2](#): the structure is clamped on the four corners marked as  $\Gamma_D$ , and the mechanical load  $\mathbf{g}$  is applied on the region  $\Gamma_N$  on the opposite side. We suppose that the load  $\mathbf{g}$  applied to  $\Gamma_N$  consists of two components: one of traction-compression (oriented along the  $x$  axis), and a vertical one (along the  $z$  axis):

$$(4.2) \quad \mathbf{g} = X\mathbf{e}_x + Z\mathbf{e}_z.$$

We suppose also that  $X$  and  $Z$  belong to the intervals  $[-\bar{g}_x, \bar{g}_x]$  and  $[-\bar{g}_z, \bar{g}_z]$  respectively. Moreover, we suppose that they are bounded by the inequality:

$$(4.3) \quad \frac{X^2}{\bar{g}_x^2} + \frac{Z^2}{\bar{g}_z^2} \leq 1.$$

The inequality (4.3) states that the set of admissible mechanical loads can be parametrized by an ellipse in  $\mathbb{R}^2$  with semi-axes equal to  $\bar{g}_x$  and  $\bar{g}_z$ .

The numerical parameters considered for this problem are reported in [Table 3](#). The simulations of this section have been performed on a Virtualbox virtual machine Linux with 1GB of dedicated memory, installed on a Dell PC equipped with a 2.80 GHz Intel i7 processor.

In order to solve the optimization problem (4.1) we consider both the polyhedral approximation approach of [section 2](#), and the method based on the subdifferential as in [section 3](#). Both methods can be applied since the set  $\mathcal{G}$  is convex, the mapping  $\mathbf{g} \mapsto \mathcal{C}(\mathbf{u}_{\Omega, \mathbf{g}}, \Omega)$  is a convex function, and the compliance operator satisfies the conditions (SA1) - (SA4) of [Proposition 3.7](#).

For the polyhedral approach, we approximated the ellipse  $\mathcal{G}$  by polygons with 4, 8, and 16 vertices denoted  $\mathcal{G}_4$ ,  $\mathcal{G}_8$ , and  $\mathcal{G}_{16}$  respectively. The polygons  $\mathcal{G}_4$ ,  $\mathcal{G}_8$ , and  $\mathcal{G}_{16}$  are defined as convex hulls of  $N$  points as follows

$$\mathcal{G}_N = \text{hull} \left\{ \left( \bar{g}_x \sin \left( \frac{2n\pi}{N} \right) \mathbf{e}_x + \bar{g}_z \cos \left( \frac{2n\pi}{N} \right) \mathbf{e}_y \right) : n \in \{0, \dots, N-1\} \right\} \subset \mathbb{R}^2.$$



FIG. 2. Structure of the 3D cantilever structure. The region  $\Gamma_N$  where the uncertain mechanical load is applied is marked in red, while the clamping region  $\Gamma_D$  is highlighted in grey.

It should be remarked that, since the compliance is invariant with respect to a change of sign in the applied load, it is necessary to consider only half of the vertices of  $\mathcal{G}_4$ ,  $\mathcal{G}_8$ , and  $\mathcal{G}_{16}$  to define the constraints of the approximated optimization problem. The structures optimized for the three cases are denoted as  $\Omega_4$  (top),  $\Omega_8$  (middle), and  $\Omega_{16}$  (bottom) respectively, and are represented in Figure 3.

In the subdifferential approach, it is necessary to identify the parameter  $\bar{\mathbf{g}}$  maximizing  $\mathcal{C}(\cdot, \Omega)$  at each step of the optimization. We can assume, by Proposition 2.1, that  $\bar{\mathbf{g}}$  belongs to the boundary of  $\mathcal{G}$ . Therefore, there exists an angle  $\alpha \in [0, 2\pi)$  such that

$$\bar{\mathbf{g}} = \sin \alpha g_x \mathbf{e}_x + \cos \alpha g_z \mathbf{e}_z.$$

Thanks to the symmetry of the compliance operator, we can restrict the search for  $\alpha$  to the interval  $[-\frac{\pi}{2}, \frac{\pi}{2})$ . The angle  $\alpha$  yielding the maximal compliance for a given shape  $\Omega$  can be identified by interpreting the compliance as a quadratic functional. Indeed, there exists a matrix  $\mathbf{M}_\Omega \in \mathbb{R}^{2 \times 2}$  such that, for all  $\hat{\alpha} \in [0, 2\pi)$ ,

$$\mathcal{C}(\mathbf{u}_{\Omega, \mathbf{g}}, \Omega) = (\sin \hat{\alpha}, \cos \hat{\alpha}) \mathbf{M}_\Omega \begin{pmatrix} \sin \hat{\alpha} \\ \cos \hat{\alpha} \end{pmatrix},$$

where the load associated to  $\mathbf{u}_{\Omega, \mathbf{g}}$  is  $\mathbf{g}(\hat{\alpha}) = \sin \hat{\alpha} g_x \mathbf{e}_x + \cos \hat{\alpha} g_z \mathbf{e}_z$ . The entries of the matrix  $\mathbf{M}_\Omega$  are

$$\begin{aligned} [\mathbf{M}_\Omega]_{11} &= m_{11} = \int_{\Omega} \boldsymbol{\sigma}(\mathbf{u}_{\Omega, \mathbf{g}_x}) : \boldsymbol{\varepsilon}(\mathbf{u}_{\Omega, \mathbf{g}_x}) \, d\mathbf{x}, \\ [\mathbf{M}_\Omega]_{22} &= m_{22} = \int_{\Omega} \boldsymbol{\sigma}(\mathbf{u}_{\Omega, \mathbf{g}_z}) : \boldsymbol{\varepsilon}(\mathbf{u}_{\Omega, \mathbf{g}_z}) \, d\mathbf{x}, \\ [\mathbf{M}_\Omega]_{12} &= [\mathbf{M}_\Omega]_{21} = m_{12} = \int_{\Omega} \boldsymbol{\sigma}(\mathbf{u}_{\Omega, \mathbf{g}_x}) : \boldsymbol{\varepsilon}(\mathbf{u}_{\Omega, \mathbf{g}_z}) \, d\mathbf{x}. \end{aligned}$$

The angle  $\alpha$  for which the maximum of the compliance is attained depends on the eigenvector related to the maximal eigenvalue of  $\mathbf{M}_\Omega$ . In particular,  $\alpha$  can be computed explicitly by the following expression

$$(4.4) \quad \alpha = \begin{cases} \frac{\pi}{4} - \frac{\beta}{2} & \text{if } m_{12} \geq 0, \\ \frac{3\pi}{4} + \frac{\beta}{2} & \text{if } m_{12} < 0, \end{cases} \quad \text{where } \beta = \arcsin \left( \frac{m_{22} - m_{11}}{2\sqrt{\left(\frac{m_{22} - m_{11}}{2}\right)^2 + m_{12}^2}} \right).$$

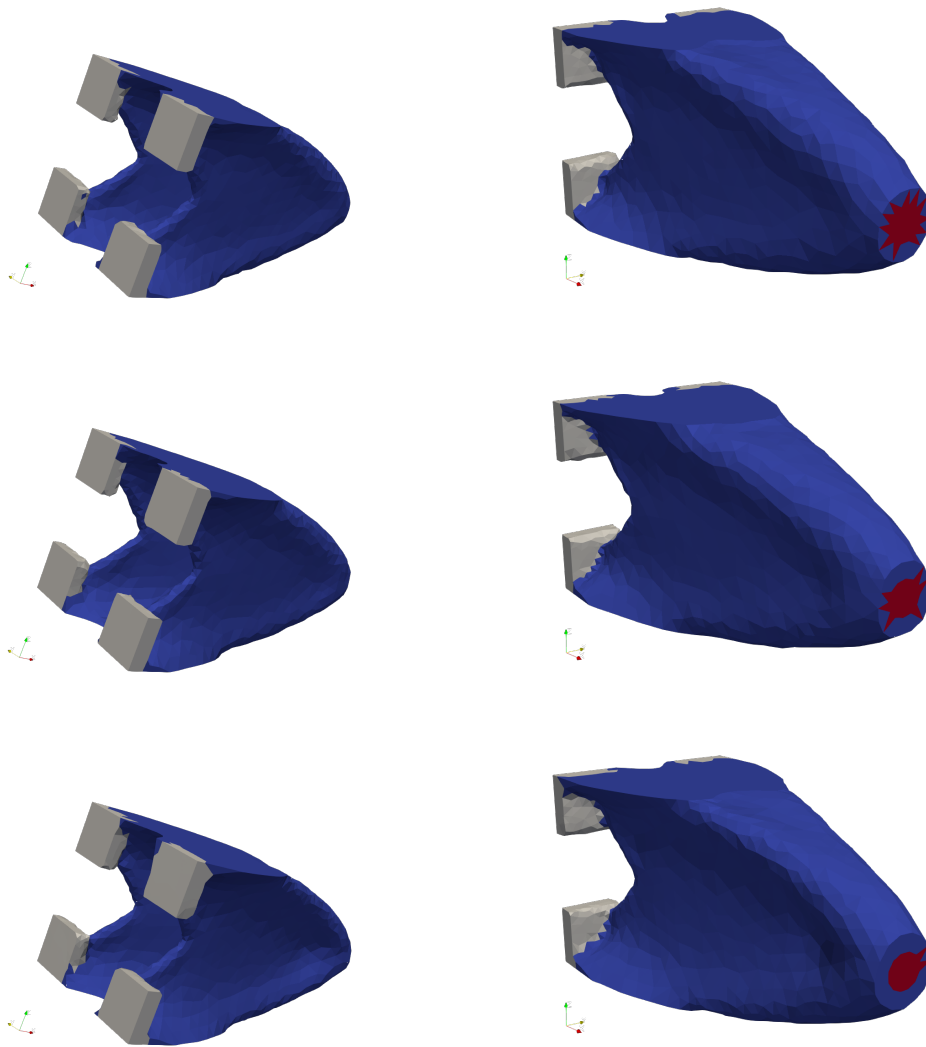


FIG. 3. Optimal shapes for the polyhedron approach with  $N = 4, 8, 16$  vertices (top to bottom).

The optimal shape resulting from the optimization based on the subdifferential is reported in [Figure 4](#), and we denote it as  $\Omega_S$ . In the graph of [Figure 5](#) is reported the evolution of the angle  $\alpha$  along the iterations. We remark that  $\alpha$  oscillates around 0, underlying the fact that vertical loads which are orthogonal to the main axis of the cantilever are responsible for the largest values of the compliance.

In [Table 1](#) we reported the numerical results of the optimization of the cantilever using the method of polyhedral approximation with three increasing degrees of precision, as well as the results of the subdifferential technique. The graph showing the progressive decrease of the volume of the structure is presented in [Figure 6a](#), while [Figure 6](#) follows the evolution of the constraint in each numerical example.

A first remark concerns the slow rate of convergence of the four examples, as



FIG. 4. Optimal shape  $\Omega_S$  resulting from the subdifferential approach.

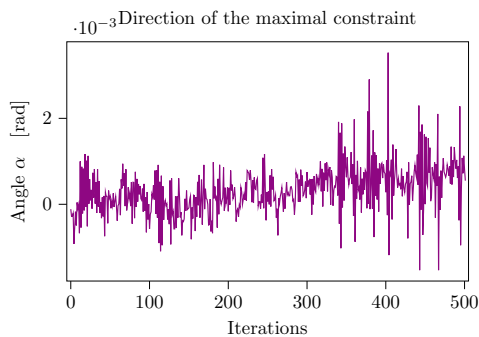


FIG. 5. Evolution of the direction of the maximal constraint (in terms of the angle  $\alpha$ ) during the optimization process.

shown in [Figure 6a](#). This issue seems to be proper to the 3D cantilever structure, as pointed out also in [\[26, Section 6.2.1\]](#). Next, we can observe in [Figure 6b](#) that in all four cases the constraint on the maximum of the compliance is satisfied. By comparing the duration of the four simulations we can state that the method based on the subdifferential is efficient and reliable to solve problem [\(4.1\)](#) since it yields a similar result as the three other simulations while requiring fewer computations of the shape derivative.

Finally, we can see that the four simulations yield similar results, as a consequence of the preeminence of the vertical load to the optimization of the structure. The fact that the Hausdorff distances between  $\Omega_N$  and  $\Omega_S$  is of the order of the mesh size for each  $N \in \{4, 8, 16\}$  supports the conclusion that all four simulations have reached a result close to the exact solution of problem [\(4.1\)](#).

**4.2. Disc.** In this section we consider the optimization of a cylinder-like structure. Once again we aim to minimize its volume, but we replace the constraint on the compliance on a constraint on the  $L^6$ -norm of the von Mises stress, which is defined as

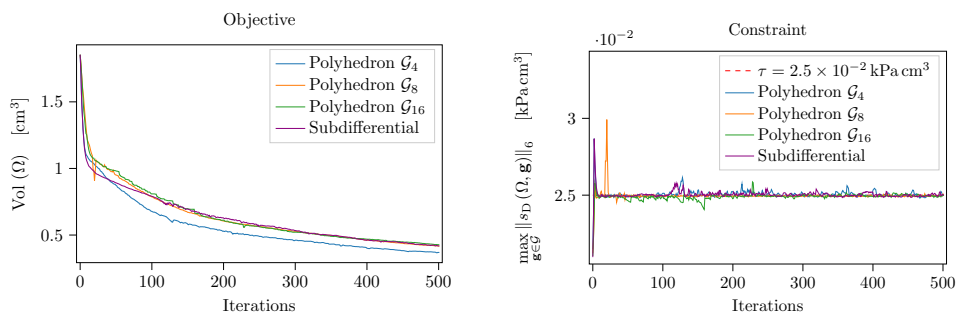
$$(4.5) \quad \|\sigma_D(\mathbf{u}_\Omega)\|_6 = \sqrt{\frac{3}{2}} \left( \int_{\Omega} (\sigma_D(\mathbf{u}_\Omega) : \sigma_D(\mathbf{u}_\Omega))^3 dx \right)^{1/6}$$

where  $\sigma_D(\mathbf{u}_\Omega) = \sigma(\mathbf{u}_\Omega) - \frac{1}{3}\mathbb{I}\text{tr}(\sigma(\mathbf{u}_\Omega))$  is the deviatoric part of the stress tensor. Refer to [\[8, 32\]](#) for more information on the physical interpretation of the von Mises

	Polyhedron			Subdifferential
	$N = 4$	$N = 8$	$N = 16$	
<b>Optimization</b>				
Duration [min]	180	187	208	180
Number of iterations	500	500	500	500
<b>Results</b>				
Final volume $\text{Vol}(\Omega)$ [ $\text{cm}^3$ ]	0.369	0.418	0.428	0.419
Maximal compliance [ $\text{Pa cm}^3$ ]	25.00	24.95	24.96	24.99
$d_H(\Omega_S, \Omega_N)$ [cm]	0.1561	0.1361	0.2130	—

TABLE 1

Numerical results for the optimization of the volume of the cantilever under constraints on the mechanical compliance, obtained using the Polyhedron method (with an increasing number of vertices), and the subdifferential method.



(a) Evolution of the objective function.

(b) Evolution of the constraint for three instances of the polyhedron method, and the subdifferential method.

FIG. 6. Convergence of the objective (volume) and the constraint (compliance) for the cantilever.

stress.

The initial condition is presented in Figure 7: the structure is fixed on a region  $\Gamma_D$  on its side, while shear loads are applied tangentially to a ring-like surface  $\Gamma_N$  on the top of the cylinder. The optimization problem to be solved is the following:

$$(4.6) \quad \left\{ \begin{array}{l} \text{Find the admissible shape } \Omega \in \mathcal{S}_{\text{adm}} \text{ minimizing the volume } \text{Vol}(\Omega) \\ \text{under the constraint } \sup_{\mathbf{g} \in \mathcal{G}} \|s_D(\mathbf{u}_\Omega)\|_6 \leq \tau, \\ \text{where the displacement } \mathbf{u}_{\Omega, \mathbf{g}} \text{ solves (1.1).} \end{array} \right.$$

Similarly to the model considered in the previous section, we suppose that the load  $\mathbf{g}$  can be written as sum of two terms, aligned with the axes  $x$  and  $y$

$$\mathbf{g} = X\mathbf{e}_x + Y\mathbf{e}_y.$$

We suppose that the intensity of the applied force is bounded by  $\bar{g}$ , so that the set of admissible loads  $\mathcal{G}$  can be parameterized by a circle in  $\mathbb{R}^2$  with radius  $\bar{g}$ . The geometric and material properties of the structure, the mesh size, the maximal value of the applied force and the threshold  $\tau$  on the  $L^6$ -norm of the von Mises stress are reported in Table 4.

Similarly to the previous section, we consider three different approximations for the polyhedral approach, where  $\mathcal{G}$  is replaced by inscribed regular polygons with  $N =$



FIG. 7. Structure of the 3D disc structure. The region  $\Gamma_N$  where the random load is applied is marked in red, while the clamping region  $\Gamma_D$  is highlighted in gray.

4, 8, and 16 vertices denoted  $\mathcal{G}_4$ ,  $\mathcal{G}_8$ , and  $\mathcal{G}_{16}$  respectively. These polygons can thus be defined as convex hulls of  $N$  points as follows

$$\mathcal{G}_N = \text{hull} \left\{ \bar{g} \left( \sin \left( \frac{2n\pi}{N} \right) \mathbf{e}_x + \cos \left( \frac{2n\pi}{N} \right) \mathbf{e}_y \right) : n \in \{0, \dots, N-1\} \right\} \subset \mathbb{R}^2.$$

Thanks to the symmetry of the constraint with respect to a change of sign in the applied force (and thus in the displacement  $\mathbf{u}_{\Omega, \mathbf{g}}$ ), only  $N/2$  constraints need to be evaluated at each step of the solution of problem (4.6). The structures resulting from applying the polyhedral approximation method are shown in Figure 8 and denoted as  $\Omega_4$ ,  $\Omega_8$ , and  $\Omega_{16}$  respectively.

Contrarily to the example discussed in subsection 4.1, the increasing refinement in the approximation of  $\mathcal{G}$  results in structures that differ significantly from one another. Indeed, we can see how  $\Omega_4$  is optimized to resist the forces applied in the directions of the four edges of  $\mathcal{G}_4$ . The structure  $\Omega_8$  (middle line of Figure 8) with eight scenarios is similar, but its four branches are wider, responding to forces oriented in the direction bisecting the main axes. Finally,  $\Omega_{16}$  (last line of Figure 8) is characterized by a rotational symmetry, thus resisting to forces applied in 16 different directions.

The similarities between the two cases allow to use a similar parametrization of the set  $\mathcal{G}$ . Let us denote  $\bar{\mathbf{g}}$  the element of  $\mathcal{G}$  maximizing the constraint functional. By the convexity of the mapping  $\mathbf{g} \mapsto \|s_D(\mathbf{u}_\Omega)\|_6$  Proposition 2.1 applies, and we deduce that  $\bar{\mathbf{g}}$  belongs to the boundary of  $\mathcal{G}$ . Thus, there exist  $\alpha \in [0, 2\pi)$  such that

$$\bar{\mathbf{g}} = \bar{g} (\sin \alpha \mathbf{e}_x + \cos \alpha \mathbf{e}_y).$$

The constraint functional considered in problem (4.6) is the  $L^6$ -norm of the von Mises stress, which is not a quadratic function. Therefore, the method used in subsection 4.1 to identify the load maximizing the constraint functional cannot be applied. Instead, we identify the value of  $\alpha$  maximizing the constraint function by applying the Newton method to the function  $\alpha \mapsto (\|s_D(\mathbf{u}_\Omega)\|_6)^6$ . It should be remarked that such a function can be expressed analytically in terms of the displacement fields generated by the application of the loads  $\bar{g}\mathbf{e}_x$  and  $\bar{g}\mathbf{e}_y$ . Thus its evaluation is extremely fast and does not require the solution of an expensive boundary value problem. Once again, thanks to the symmetry of the constraint under a change of sign of the mechanical

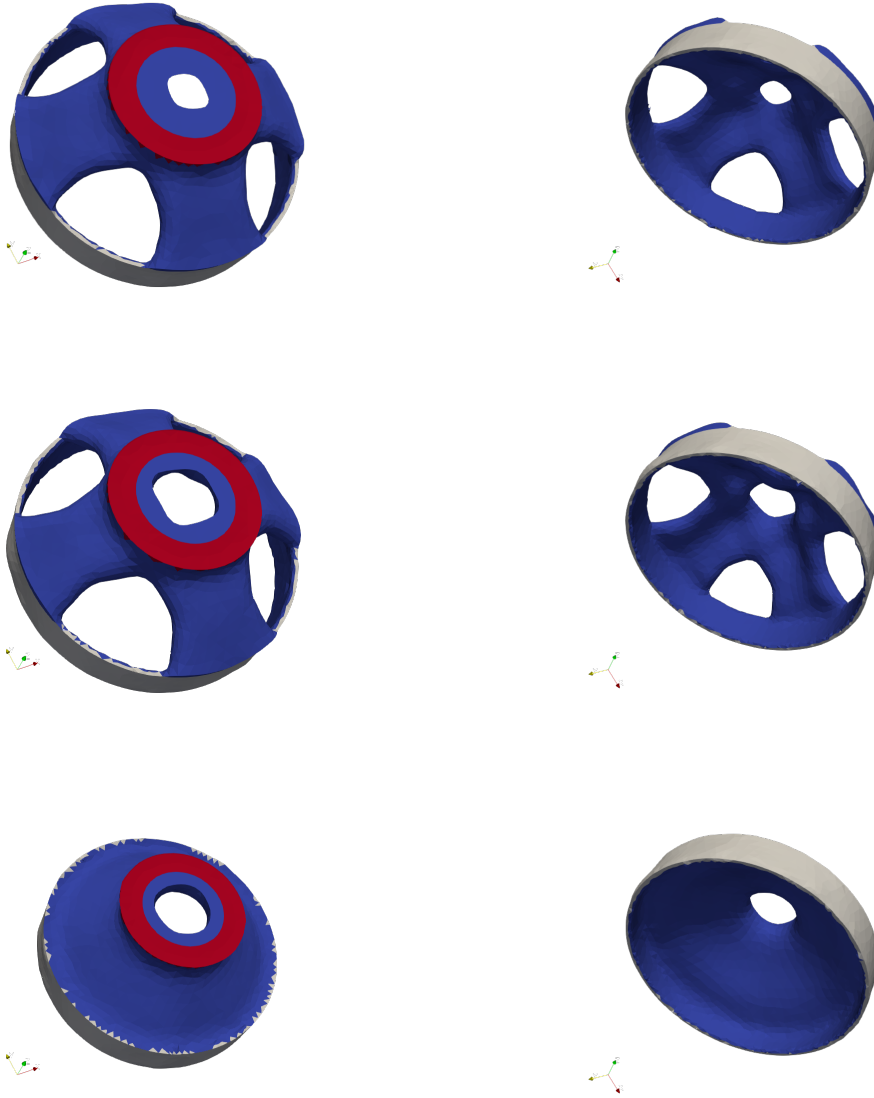


FIG. 8. *Optimal shape for the polyhedron approach with  $N = 4, 8, 16$  vertices from top to bottom.*

load, the search of the critical direction  $\alpha$  can be limited to the interval  $[-\frac{\pi}{2}, \frac{\pi}{2})$ . The shape  $\Omega_S$  resulting from the application of the subdifferential approach is reported in [Figure 9](#).

The numerical results of the optimization performed using the polyhedral approximation and the subdifferential method are reported in [Table 2](#). In [Figure 10](#) we plotted the value of the maximal constraint throughout the optimization: firstly for the three instances of the polyhedral approximation algorithm ([Figure 10a](#)), next comparing them with the evolution of the constraints for the subdifferential approach



FIG. 9. *Optimal shape  $\Omega_S$  resulting from the Subdifferential approach.*

(Figure 10b). The trend of the objective function for all four simulations is represented in Figure 11a. In Figure 11b we report the evolution of the angle  $\alpha$  parametrising the direction of the load maximizing the  $L^6$ -norm of the von Mises stress at each step.

The method of subdifferential yields an optimal structure  $\Omega_S$  with rotational symmetry similar to the most precise polyhedral approximation  $\Omega_{16}$ , as shown by Figure 9. If we assume that  $\Omega_S$  is representative of the exact solution of problem (4.6), the comparison of the illustrations of the optimal shapes validates the convergence result of Theorem 2.9. Indeed, the similarity between  $\Omega_N$  and  $\Omega_S$  increases when  $\mathcal{G}_N$  approximates better the original set  $\mathcal{G}$ . This statement is corroborated by the numerical computation of the Hausdorff distances between  $\Omega_S$  and the shapes resulting from the polyhedral approximation, as shown in Table 2.

By looking at the graph of Figure 10b we remark that the constraint on the maximum of the  $L^6$ -norm of the von Mises stress is overall satisfied by the method of subdifferential, but more significant perturbations can be observed. A more difficult convergence compared to the polyhedron method can be remarked in Figure 11a, where a slower decrease in the objective function is evident, to the point that a larger number of iterations has been necessary in order to reach a stable configuration (200 for the polyhedron method and 300 for the subdifferential). Both issues are justified by the rotational symmetry of the optimization problem. As the graph in 11b shows, the critical direction  $\alpha$  varies widely at each step of the optimization algorithm, even from one iteration to the next.

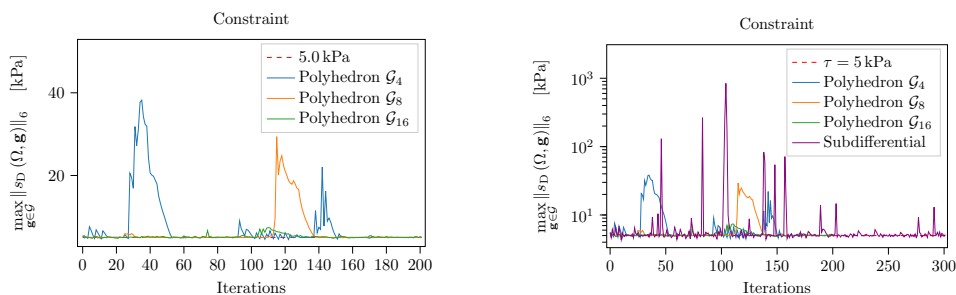
By comparing the duration of the simulations as presented in Table 2, we remark that the subdifferential approach is overall faster than the polyhedral approximation, since it requires fewer evaluations of the constraint functional. Therefore, the shorter duration of each step compensates the smaller contribution of each iteration to the decrease of the objective function.

**5. Conclusions and perspectives.** In this paper we have compared two different methods for solving shape optimization problems under worst-case constraints on a given function. The first method can only be applied to convex functions of the displacement, and is based on the approximation of the set  $\mathcal{G}$  of admissible loads by polyhedra. This method is effectively the design of a structure that satisfies the constraint in a finite number of representative load cases. The second method is based on the calculation of an element of the subdifferential of the constraint by identifying

	Polyhedron			Subdifferential
	$N = 4$	$N = 8$	$N = 16$	
<b>Execution of the optimization</b>				
Duration of the optimization [min]	189	296	499	159
Number of iterations	200	200	200	300
<b>Results</b>				
Final volume $\text{Vol}(\Omega)$ [ $\text{cm}^3$ ]	666.27	692.18	751.46	874.07
Maximal von Mises stresses [kPa]	5.015	5.053	5.164	5.183
$d_H(\Omega_S, \Omega_N)$ [cm]	3.001	3.037	1.347	—

TABLE 2

Numerical results for the optimization of the volume of a disc structure under constraints on the  $L^6$ -norm of the von Mises stress, obtained using the Polyhedron method (with an increasing number of vertices), and the Subdifferential method.



(a) Evolution of the constraint for three instances of the polyhedron method (4, 8, and 16 vertices respectively).

(b) Evolution of the constraint for three instances of the Polyhedron method, and the Subdifferential method.

FIG. 10. Convergence of the constraint ( $L^6$ -norm of the von Mises stress) for the disc structure.

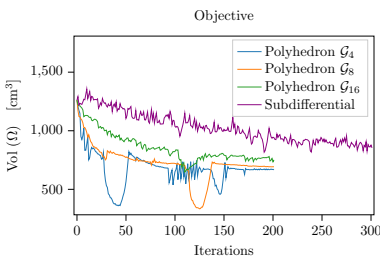
the critical element of the  $\mathcal{G}$  that maximizes the constraint and differentiating in the relative direction.

The numerical simulations of section 4 support the effectiveness of both methods in the case of an admissible set of loads parameterized by an ellipse in  $\mathbb{R}^2$ . We observed that in both cases the subdifferential method is faster than the polyhedral approximation, since it requires fewer evaluations of the constraint function. However, we note that when the allowable load maximizing the constraint is not unique, the convergence of the subdifferential method is degraded and smaller and more numerous optimization steps are required to converge.

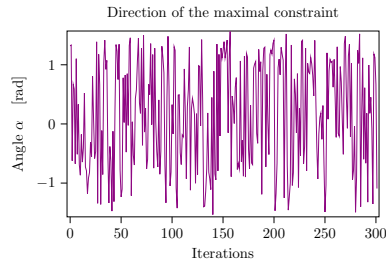
One way to improve the subdifferential method is to consider multiple elements of the subdifferential of the constraint function. Such a variant of the algorithm would require identifying whether multiple mechanical loads maximize the constraint for a given shape. A possible direction of development could be the adaptation of the proximal algorithm to shape optimization, since it already relies on the subdifferential in the sense of Clarke. See [6, 35] and references therein for further information on the proximal algorithm in non-smooth optimization.

## REFERENCES

- [1] Samir Adly, Loïc Bourdin, Fabien Caubet, and Aymeric Jacob de Cordemoy. Shape Optimization for Variational Inequalities: The Scalar Tresca Friction Problem. *SIAM Journal on Optimization*, pages 2512–2541, December 2023.



(a) Evolution of the objective function.



(b) Evolution of the direction of the maximal constraint (in terms of the angle  $\alpha$ ) during the optimization process.

FIG. 11. Convergence of the objective (volume) for the Polyhedron and Subdifferential methods, and direction of the largest constraint under the Subdifferential method for the disc structure.

- [2] Grégoire Allaire and Charles Dapogny. A linearized approach to worst-case design in parametric and geometric shape optimization. *Mathematical Models and Methods in Applied Sciences*, 24(11):2199–2257, October 2014.
- [3] Grégoire Allaire and Charles Dapogny. A deterministic approximation method in shape optimization under random uncertainties. *SMAI Journal of Computational Mathematics*, 1:83–143, 2015.
- [4] Grégoire Allaire and François Jouve. A level-set method for vibration and multiple loads structural optimization. *Computer Methods in Applied Mechanics and Engineering*, 194(30):3269–3290, August 2005.
- [5] Samuel Amstutz and Marc Ciligot-Travaïn. A notion of compliance robustness in topology optimization. *ESAIM: Control, Optimisation and Calculus of Variations*, 22(1):64–87, January 2016.
- [6] Hedy Attouch and Jérôme Bolte. On the convergence of the proximal algorithm for nonsmooth functions involving analytic features. *Mathematical Programming*, 116(1):5–16, January 2009.
- [7] Hedy Attouch and Roger J.-B. Wets. Quantitative Stability of Variational Systems: I. The Epigraphical Distance. *Transactions of the American Mathematical Society*, 328(2):695–729, 1991.
- [8] G. Augusti, J. B. Martin, and W. Prager. On the Decomposition of Stress and Strain Tensors into Spherical and Deviatoric Parts. *Proceedings of the National Academy of Sciences of the United States of America*, 63(2):239–241, 1969.
- [9] I. Bárány and Z. Füredi. Approximation of the Sphere by Polytopes having Few Vertices. *Proceedings of the American Mathematical Society*, 102(3):651–659, 1988.
- [10] Aharon Ben-Tal, Laurent El Ghaoui, and Arkadi Nemirovski. Robust Optimization. In *Robust Optimization*. Princeton University Press, August 2009.
- [11] Aharon Ben-Tal and Arkadi Nemirovski. Robust optimization – methodology and applications. *Mathematical Programming*, 92(3):453–480, May 2002.
- [12] Fabien Caubet, Marc Dambrine, and Rajesh Mahadevan. Shape derivative for some eigenvalue functionals in elasticity theory. *SIAM J. Control Optim.*, 59(2):1218–1245, 2021.
- [13] Fabien Caubet, Marc Dambrine, and Rajesh Mahadevan. Shape Sensitivity of Eigenvalue Functionals for Scalar Problems: Computing the Semi-derivative of a Minimum. *Applied Mathematics & Optimization*, 86(1):10, June 2022.
- [14] Shikui Chen, Wei Chen, and Sanghoon Lee. Level set based robust shape and topology optimization under random field uncertainties. *Structural and Multidisciplinary Optimization*, 41(4):507–524, April 2010.
- [15] Denise Chenaïs. On the existence of a solution in a domain identification problem. *Journal of Mathematical Analysis and Applications*, 52(2):189–219, November 1975.
- [16] Elena Cherkvaev and Andrej Cherkvaev. Principal Compliance and Robust Optimal Design. *Journal of Elasticity*, 72(1):71–98, July 2003.
- [17] Frank H. Clarke. *Optimization and Nonsmooth Analysis*. Classics in Applied Mathematics. Society for Industrial and Applied Mathematics, 1990.
- [18] Marc Dambrine, Charles Dapogny, and Helmut Harbrecht. Shape optimization for quadratic

- functionals and states with random right-hand sides. *SIAM J. Control Optim.*, 53(5):3081–3103, 2015.
- [19] Marc Dambrine, Helmut Harbrecht, and Benedicte Puig. Incorporating knowledge on the measurement noise in electrical impedance tomography. *ESAIM Control Optim. Calc. Var.*, 25:Paper No. 84, 16, 2019.
- [20] Marc Dambrine, Djalil Kateb, and Jimmy Lamboley. An extremal eigenvalue problem for the Wentzell–Laplace operator. *Annales de l’Institut Henri Poincaré C, Analyse non linéaire*, 33(2):409–450, March 2016.
- [21] Marc Dambrine and Antoine Laurain. A first order approach for worst-case shape optimization of the compliance for a mixture in the low contrast regime. *Struct. Multidiscip. Optim.*, 54(2):215–231, 2016.
- [22] Marc Dambrine and Salah Zerrouq. Robust inverse homogenization of elastic microstructures. *Journal of Optimization Theory and Applications*, 199(1):209 – 232, 2023.
- [23] John M. Danskin. The Theory of Max-Min, with Applications. *SIAM Journal on Applied Mathematics*, 14(4):641–664, 1966.
- [24] Frédéric de Gournay, Grégoire Allaire, and François Jouve. Shape and topology optimization of the robust compliance via the level set method. *ESAIM: Control, Optimisation and Calculus of Variations*, 14(1):43–70, January 2008.
- [25] Michel C. Delfour and Jean-Paul Zolesio. *Shapes and Geometries: Metrics, Analysis, Differential Calculus, and Optimization, Second Edition*. Advances in Design and Control. SIAM, Philadelphia, siam edition, January 2011.
- [26] Florian Feppon. *Optimisation Topologique de Systèmes Multiphysiques*. PhD thesis, Université Paris Saclay (COMUE), December 2019.
- [27] Florian Feppon, Grégoire Allaire, and Charles Dapogny. Null space gradient flows for constrained optimization with applications to shape optimization. *ESAIM: Control, Optimisation and Calculus of Variations*, 26:90, 2020.
- [28] Kang Gao, Duy Minh Do, Sheng Chu, Gang Wu, H. Alicia Kim, and Carol A. Featherston. Robust topology optimization of structures under uncertain propagation of imprecise stochastic-based uncertain field. *Thin-Walled Structures*, 175:109238, June 2022.
- [29] Xu Guo, Weisheng Zhang, and Li Zhang. Robust structural topology optimization considering boundary uncertainties. *Computer Methods in Applied Mechanics and Engineering*, 253:356–368, January 2013.
- [30] Abderrahmane Habbal. Nonsmooth Shape Optimization Applied to Linear Acoustics. *SIAM Journal on Optimization*, 8(4):989–1006, November 1998.
- [31] Antoine Henrot and Michel Pierre. *Shape Variation and Optimization: A Geometrical Analysis*. Number 28 in Tracts in Mathematics. European Mathematical Society, Zurich, 2018.
- [32] Robert Millard Jones. *Deformation Theory of Plasticity*. Bull Ridge Corporation, Blacksburg, Virginia, 2008.
- [33] Toni Lassila, Andrea Manzoni, Alfio Quarteroni, and Gianluigi Rozza. Boundary control and shape optimization for the robust design of bypass anastomoses under uncertainty. *ESAIM: Mathematical Modelling and Numerical Analysis*, 47(4):1107–1131, July 2013.
- [34] Daniel Luft, Volker H. Schulz, and Kathrin Welker. Efficient Techniques for Shape Optimization with Variational Inequalities Using Adjoints. *SIAM Journal on Optimization*, 30(3):1922–1953, January 2020.
- [35] Dominikus Noll. Convergence of Non-smooth Descent Methods Using the Kurdyka–Lojasiewicz Inequality. *Journal of Optimization Theory and Applications*, 160(2):553–572, February 2014.
- [36] Ralph Tyrell Rockafellar. *Convex Analysis*. Princeton Mathematical Series. Princeton University Press, 1970.

**Appendix A. Parameters for the numerical experiments.**

<b>Geometry of the structure</b>		
cross section length	$\ell_s$	1.0 cm
longitudinal length	$\ell_x$	2.0 cm
sidelength of $\Gamma_D$		0.3 cm
radius of $\Gamma_N$		0.1 cm
<b>Elastic coefficients</b>		
young's modulus	$E$	200 MPa
poisson's ratio	$\nu$	0.3
<b>Mechanical loads</b>		
compression load	$\bar{g}_x$	25 kPa
vertical load	$\bar{g}_z$	10 kPa
<b>Mesh size parameters</b>		
minimal mesh size	<b>hmin</b>	0.025 cm
maximal mesh size	<b>hmax</b>	0.10 cm
<b>Thresholds for the inequality constraints</b>		
threshold on the compliance	$\tau$	$2.5 \times 10^{-2}$ kPa cm <sup>3</sup>
bound on the probability of failure	$\bar{p}$	1.0%

TABLE 3

Numerical data concerning the geometry and the mechanics of the cantilever of [Figure 2](#).

<b>Geometry of the structure</b>		
height of the domain		12.0 cm
maximal radius of the romain		12.0 cm
<b>Region <math>\Gamma_N</math></b>		
inner radius of $\Gamma_N$		4.0 cm
outer radius of $\Gamma_N$		6.0 cm
<b>Region <math>\Gamma_D</math></b>		
thickness of $\Gamma_D$		2.0 cm
<b>Mesh size parameters</b>		
minimal mesh size	<b>hmin</b>	0.75 cm
maximal mesh size	<b>hmax</b>	1.25 cm
<b>Elastic coefficients</b>		
Young's modulus	$E$	200 MPa
Poisson's ratio	$\nu$	0.3
<b>Mechanical loads</b>		
maximal load in any direction	$\bar{g}$	10 kPa
threshold on $\ s_D\ _6$	$\tau$	5.0 kPa

TABLE 4

Numerical data concerning the geometry and the mechanics of the disc structure of [Figure 7](#).